



HAL
open science

Iterative wave-front reconstruction in the Fourier domain

Charlotte Z. Bond, Carlos Correia, Jean-Francois Sauvage, Benoit Neichel,
Thierry Fusco

► **To cite this version:**

Charlotte Z. Bond, Carlos Correia, Jean-Francois Sauvage, Benoit Neichel, Thierry Fusco. Iterative wave-front reconstruction in the Fourier domain. *Optics Express*, 2017, 25 (10), p. 11452-11465. 10.1364/OE.25.011452 . hal-01653279

HAL Id: hal-01653279

<https://hal.science/hal-01653279>

Submitted on 1 Dec 2017

HAL is a multi-disciplinary open access archive for the deposit and dissemination of scientific research documents, whether they are published or not. The documents may come from teaching and research institutions in France or abroad, or from public or private research centers.

L'archive ouverte pluridisciplinaire **HAL**, est destinée au dépôt et à la diffusion de documents scientifiques de niveau recherche, publiés ou non, émanant des établissements d'enseignement et de recherche français ou étrangers, des laboratoires publics ou privés.

Iterative wave-front reconstruction in the Fourier domain

CHARLOTTE Z. BOND,^{1*} CARLOS M. CORREIA,¹ JEAN-FRANÇOIS SAUVAGE,^{1,2} BENOIT NEICHEL,¹ AND THIERRY FUSCO^{1,2}

¹Aix Marseille Universite, CNRS, LAM (Laboratoire d'Astrophysique de Marseille) UMR 7326, 13388, Marseille, France

²ONERA (Office National d'Etudes et de Recherches Aérospatiales), B.P. 72, F-92322 Châtillon, France
*charlotte.bond@lam.fr

Abstract: The use of Fourier methods in wave-front reconstruction can significantly reduce the computation time for large telescopes with a high number of degrees of freedom. However, Fourier algorithms for discrete data require a rectangular data set which conform to specific boundary requirements, whereas wave-front sensor data is typically defined over a circular domain (the telescope pupil). Here we present an iterative Gerchberg routine modified for the purposes of discrete wave-front reconstruction which adapts the measurement data (wave-front sensor slopes) for Fourier analysis, fulfilling the requirements of the fast Fourier transform (FFT) and providing accurate reconstruction. The routine is used in the adaptation step only and can be coupled to any other Wiener-like or least-squares method. We compare simulations using this method with previous Fourier methods and show an increase in performance in terms of Strehl ratio and a reduction in noise propagation for a 40×40 SPHERE-like adaptive optics system. For closed loop operation with minimal iterations the Gerchberg method provides an improvement in Strehl, from 95.4% to 96.9% in K-band. This corresponds to ~ 40 nm improvement in rms, and avoids the high spatial frequency errors present in other methods, providing an increase in contrast towards the edge of the correctable band.

© 2017 Optical Society of America

OCIS codes: (070.0070) Fourier optics and signal processing; (100.0100) Image processing; (000.4430) Numerical approximation and analysis; (010.1080) Active or adaptive optics; (010.7350) Wave-front sensing.

References and links

1. T. de Zeeuw, R. Tamai, and J. Liske, "Constructing the E-ELT," <http://www.eso.org/sci/facilities/eelt/docs/>, (2014).
2. The TMT Observatory Corporation, "Thirty meter telescope construction proposal," <http://www.tmt.org/news/TMT-ConstructionProposal-Public.pdf>, (2007).
3. GMTO Corporation, "Giant magellan telescope scientific promise and opportunities," http://www.gmto.org/Resources/GMT-SCI-REF-00482_2_GMT_Science_Book.pdf, (2012).
4. I. Montilla, C. Béchet, M. LeLouarn, C. Correia, M. Tallon, M. Reyes, and E. Thiébut, "Comparison of reconstruction and control algorithms on the ESO end-to-end simulator OCTOPUS," in "AO4ELT-I", 03002, (2010).
5. R. L. Frost, C. K. Rushforth, and B. S. Baxter, "Fast FFT-based algorithm for phase estimation in speckle imaging," *Appl. Opt.* **18**, 2056–2061 (1979).
6. K. R. Freischlad and C. L. Koliopoulos, "Wavefront reconstruction from noisy slope or difference data using the discrete Fourier transform," *Proc. SPIE* 0551, 74 (1986).
7. F. Roddier and C. Roddier, "Wavefront reconstruction using iterative Fourier transforms," *Appl. Opt.* **30**, 1325–1327 (1991).
8. C. M. Correia and J. Teixeira, "Anti-aliasing Wiener filtering for wave-front reconstruction in the spatial-frequency domain for high-order astronomical adaptive-optics systems," *J. Opt. Soc. Am. A* **31**, 2763–2774 (2014).
9. L. A. Poyneer, D. T. Gavel, and J. M. Brase, "Fast wave-front reconstruction in large adaptive optics systems with use of the Fourier transform," *J. Opt. Soc. Am. A* **19**, 2100–2111 (2002).
10. L. A. Poyneer, "Advanced techniques for Fourier transform wavefront reconstruction," *Proc. SPIE* 4839, 1023–1034 (2003).
11. E. N. Ribak, Y. Carmon, A. Talmi, O. Glazer, O. Srour, and N. Zon, "Full wave front reconstruction in the Fourier domain," *Proc. SPIE* 6272, 627254 (2006).
12. C. Correia, C. Kulcsar, J.-M. Conan, and H.-F. Raynaud, "Hartmann modelling in the discrete spatial-frequency domain: application to real-time reconstruction in adaptive optics," *Proc. SPIE* 7015, 701551 (2008).

13. L. A. Poyneer and J.-P. Véran, "Optimal modal Fourier-transform wavefront control," *J. Opt. Soc. Am. A* **22**, 1515–1526 (2005).
14. K. R. Freischlad and C. L. Koliopoulos, "Modal estimation of a wave front from difference measurements using the discrete Fourier transform," *J. Opt. Soc. Am. A* **3**, 1852–1861 (1986).
15. K. R. Freischlad, "Wave-front integration from difference data," *Proc. SPIE* **1755**, 212 (1993).
16. R. W. Gerchberg, "Super-resolution through error energy reduction," *Optica Acta* **21**, 709–720 (1974).
17. P. Chatterjee, S. Mukherjee, S. Chaudhuri, and G. Seetharaman, "Application of Papoulis-Gerchberg method in image super-resolution and inpainting," *The Computer Journal* **52**, 80–89 (2007).
18. T. Fusco, G. Rousset, J.-F. Sauvage, C. Petit, J.-L. Beuzit, K. Dohlen, D. Mouillet, J. Charton, M. Nicolle, M. Kasper, P. Baudoz, and P. Puget, "High-order adaptive optics requirements for direct detection of extrasolar planets: application to the SPHERE instrument," *Opt. Express* **14**, 7515–7534 (2006).
19. R. Conan and C. Correia, "Object-oriented Matlab adaptive optics toolbox," *Proc. SPIE* **9148**, 91486C (2014).
20. W. Zou and J. P. Rolland, "Quantifications of error propagation in slope-based wavefront estimations," *J. Opt. Soc. Am. A* **23**, 2629–2638 (2006).
21. F. Rigaut, J.-P. Véran, and O. Lai, "An analytical model for Shack-Hartmann based adaptive optics systems," *Proc. SPIE* **3353**, 1038 (1998).
22. J. W. Hardy, "Adaptive Optics for Astronomical Telescopes" (Oxford University Press, 1998).
23. A. Niranjana, "HARMONI: the first light integral field spectrograph for the E-ELT," in "Proc. SPIE 9147", Ground-based and Airborne Instrumentation for Astronomy V, 914725, (2014).

1. Introduction

The performance of large ground-based telescopes depends on the ability of adaptive optics (AO) systems to correct for phase distortions caused by atmospheric turbulence. This is highly dependent on the accuracy of the wave-front measurements provided by the AO systems wave-front sensor and the speed at which the wave-front is measured and corrected. Therefore an accurate high speed wave-front reconstruction algorithm is highly desirable.

Future Extremely Large Telescopes (ELTs) are in the design process [1–3]. These large facilities will incorporate complex AO systems with a very high number of degrees of freedom, specifically the number of correctable spatial modes $\sim 5 \times 10^3$. To provide a high rate of correction (in the kHz regime) very fast wave-front reconstruction algorithms are required. Standard wavefront reconstruction requires $N \times N$ operations, with N being the number of correctable modes to solve for the linear system of equations that is customarily used. Use of Fast Fourier Transforms (FFTs) can in principle reduce the number of operations to $N \log(N)$, providing a vast improvement in the speed of the reconstruction process [4]. For an ELT sized system this is a potential reduction in the number of operations by 3 orders of magnitude.

Initial attempts to use Fourier methods for wave-front reconstruction [5, 6] did not take into account the telescope pupil imposed on the data, applying such methods to data defined over a rectangular domain. In [7] the issue of an arbitrary data boundary, such as the pupil, is addressed with the proposition of a Gerchberg-like algorithm to extrapolate the known data beyond the boundary and simultaneously reconstruct the phase. The routine employs the use of the Laplacian of the data, $\nabla^2 = \partial^2/\partial x^2 + \partial^2/\partial y^2$, in the continuous Fourier domain leading to a simple, complex multiplication for reconstruction of the phase $\hat{\phi} = (\kappa_x \tilde{s}_x + \kappa_y \tilde{s}_y) / (2i\pi|\kappa|^2)$ where $\hat{\phi}$ is the reconstructed phase in Fourier space, κ is the spatial-frequency vector and \tilde{s} are slopes in Fourier space. However, this fails to take into account a more realistic measurement process, particularly the discrete nature of the wave-front measurement in terms of lenslet sampling and the pixelated WFS spots on the detector, and to justify the use of the Laplacian as the solution of a least-squares minimisation of the reconstruction process [8]. Additional works have developed other Fourier methods for wave-front reconstruction based on satisfying the boundary conditions of the FFT [9–11].

In this paper we expand on the methods presented in [7, 12], reconstructing the wave-front using Fourier filters derived from discrete models of the measurement process, as developed in [8]. We include additional constraints, specifically enforcing periodicity on the WFS data and demonstrate the improvements offered by this routine using open and closed loop end-to-end

simulations of an adaptive optics system using a Shack-Hartmann WF sensor. The specific motivation is to provide a robust reconstruction in the Fourier domain in order to investigate anti-aliasing filters developed in [8]. To observe the anticipated gains in contrast we require accurate reconstructors which perform well across the correction band, and particularly avoid errors at high spatial frequencies.

2. Reconstruction in the Fourier domain

The description of the wave-front measurement process can be approximated by a series of convolutions in direct space (the *forward model*). In the Fourier domain this translates to a series of multiplications [8]:

$$\tilde{\mathbf{s}}(\boldsymbol{\kappa}) = \tilde{G}\tilde{\phi}(\boldsymbol{\kappa}) + \tilde{\boldsymbol{\eta}} \quad (1)$$

where $\boldsymbol{\kappa} = \{\kappa_x, \kappa_y\}$ is the bi-dimensional spatial frequency vector, $\tilde{\mathbf{s}}$ is the slope measurement, \tilde{G} describes the slope measurement for given phase, $\tilde{\phi}$ is the phase and $\tilde{\boldsymbol{\eta}}$ is the measurement noise. $\tilde{\cdot}$ denotes a variable in the Fourier space.

Wave-front reconstruction in the Fourier domain is achieved using filters, \tilde{R} , which convert the measured slopes into a reconstructed phase:

$$\tilde{\phi} = \tilde{R}_x\tilde{\mathbf{s}}_x + \tilde{R}_y\tilde{\mathbf{s}}_y \quad (2)$$

The inverse Fourier transform of $\tilde{\phi}$ gives the reconstructed phase in direct space, $\hat{\phi}$. The construction of \tilde{R} depends on the measurement model used and various filters have previously been constructed based on different wave-front sensor geometries [8, 12–14]. The general form of such a filter is a Wiener filter, the Fourier equivalent of a direct space minimum-mean-squared-error (MMSE) method, which minimises the residual error variance and maximises the Strehl:

$$\tilde{R} = \frac{\tilde{G}^*}{|\tilde{G}|^2 + \gamma \frac{W_{\boldsymbol{\eta}}}{W_{\phi}}} \quad (3)$$

$W_{\boldsymbol{\eta}}$ is the power spectral density (PSD) of the noise in the measurement and W_{ϕ} is the PSD of the turbulent phase. * represents complex conjugate variables. γ is a constant with $\gamma = 0$ representing a least squares (LSQ) reconstruction and $\gamma = 1$ the MMSE. In the results presented here we consider the MMSE filter.

Equation (3) shows that the solution for Fourier reconstruction involves the division by $|\tilde{G}|^2$, which in continuous space is equal to $\kappa_x^2 + \kappa_y^2$, and equivalent to the formulation involving the Laplacian proposed by Roddier&Roddier [7]. We consider the filters developed in [8] which take into account the discrete measurement process. These correspond to the following direct space measurement model of the Shack-Hartmann:

$$G = \text{|||} \left(\frac{\mathbf{x}}{d} \right) \times \left[\Pi \left(\frac{\mathbf{x}}{d} \right) \otimes \nabla \right] \quad (4)$$

where d is the lenslet spacing, ∇ is the gradient function, \times represents a simple multiplication and \otimes is a convolution. The comb function, $\text{|||} \left(\frac{\mathbf{x}}{d} \right)$, represents the lenslet sampling and manifests itself as an aliasing factor in the Fourier domain. The convolution with the square function, $\Pi \left(\frac{\mathbf{x}}{d} \right)$, represents the process by which the gradients are averaged in the Shack-Hartmann measurement: each measurement is the difference between the average phase across the opposite edges of the lenslet. A subtle correction to the formalism of Eq. (4) as derived in [8] is that the difference is effectively taken over $d - d_{px}$, where d_{px} is the length of one pixel on the WFS detector. This averaging process is represented in the Fourier domain as multiplications by sinc functions.

3. Adapting to the aperture of the telescope

3.1. Limitations of Fourier analysis for non-rectangular domains

The Fourier transform decomposes a function into Fourier modes, with these modes satisfying the conditions of an orthonormal basis over an infinite cartesian space. Analysis of discrete data defined over a finite space, such as slope measurements from a WFS, requires the Fast Fourier Transform (FFT). The Fourier modes used in the FFT are defined by the interval and sampling of the data. The FFT requires data defined over a rectangular space and assumes that the data is periodic. In this way the data can be completely described by the FFT modes. If either of these two conditions are not full-filled errors can occur in the Fourier analysis.

In the case of adaptive optics systems the data is the slope measurements from a wave-front sensor. The telescope aperture is superimposed on this data and therefore valid measurements do not fill a rectangular space. The sharp cut-off imposed by the aperture is interpreted by numerical FT algorithms as additional frequency components which do not represent the frequency content of the slope measurement but rather the convolution, in Fourier space, with the pupil function. This leads to large errors in the frequency content which propagate through the reconstruction process, resulting in large errors in the estimated phase [9].

3.2. Extending wave-front sensor data

To avoid the errors induced by the imposition of the pupil the wave-front sensor data must be extended outside the aperture, conforming to the periodic conditions required by the FFT and the characteristics of the wave-front sensor data [6, 15]. These conditions can be characterised by two constraints:

1. $\frac{1}{D} \int_D \nabla \phi \, d\mathbf{x} = 0$. If the phase is spatially periodic then the integral of the gradients across the data set must be zero. Numerically this means the sum of each row (for x slopes) and each column (for y slopes) is equal to zero. This can be imposed during the slope extension as follows [9]:

$$\begin{aligned} s_x(m, N) &= -\sum_{n=1}^{N-1} s_x(m, n) & 1 \leq m \leq N \\ s_y(N, n) &= -\sum_{m=1}^{N-1} s_y(m, n) & 1 \leq n \leq N \end{aligned} \quad (5)$$

2. $\text{rot}(\nabla \phi) = 0$. If the phase is spatial continuous then the curl of the gradient is zero and any closed path sum of gradients must equal zero.

As both constraints are derived from a continuous noise-less approach they may be impacted by noise in the measurement and the discrete nature of the measurement.

Two methods proposed in [9] suggest extending the data by extrapolating the gradients at the edges of the aperture, conforming to the constraints identified above. The *extension method* defined in [9], here referred to as the *Hudgin extension*, extends the slopes by repeating the gradients at the edge of the aperture until the rectangular data boundary is reached. The x slopes are extended up and down from the aperture and the y slopes are extended left and right. The periodic condition is then explicitly imposed. In this paper periodicity is always enforced when the Hudgin extension is used.

Methods of extending the data such as the Hudgin extension have demonstrated good reconstruction and an avoidance of the large errors due to the imposition of the aperture. However, they only extrapolate from the data at the edges which will be most impacted by noise on account of partial illumination of the sub-apertures. Our aim is to devise an extension method which extrapolates the overall characteristics of the data within the aperture. Here we propose a new extension method based on an iterative Gerchberg process in the Fourier domain, as previously suggested in [12].

3.3. Gerchberg method

The Gerchberg routine is designed to extend known data outside the measurement bounds, using Fourier analysis to extrapolate the data and retain the Fourier properties of the known data over an extended region. Originally proposed by Gerchberg in 1974 [16] as a method for extending spectra to enhance resolution, it can be applied to WFS data to extend beyond the bounds of the aperture. An instructive illustration of the Gerchberg method applied to 1D data is shown in [17].

For our purposes the Gerchberg routine has been adapted for wave-front reconstruction using the Fourier measurement filters. The filter replaces the band-width restriction in the general Gerchberg algorithm [17] (the low pass filter). The first step takes the Fourier transform of the raw slope data. Then the phase is reconstructed in Fourier space:

$$\hat{\phi} = \frac{\tilde{G}_x^* \tilde{s}_x + \tilde{G}_y^* \tilde{s}_y}{|\tilde{G}_x|^2 + |\tilde{G}_y|^2} \quad (6)$$

In this step the phase is reconstructed using a filter equivalent to a least squares approach (i.e. no noise PSD component in the denominator, see Eq. (3)). Within the Gerchberg routine the filter is applied for each iteration. Inclusion of the noise term (equivalent to an MMSE approach) for recursive filtering leads to an over-filtering of the noise and potential large errors in the extended data. Subsequently the MMSE filter is only used for the final phase reconstruction.

Using the measurement filter (\tilde{G}) the slopes are estimated from the reconstructed phase and an inverse Fourier transform returns the estimated slopes in direct space:

$$\hat{s} = \tilde{G} \hat{\phi} \quad \longrightarrow \quad \hat{s} = \tilde{\mathcal{F}}^{-1}(\hat{\phi}) \quad (7)$$

The final slopes estimate takes the original measurement within the pupil and the estimated slopes outside the pupil. The Gerchberg process is then repeated as necessary, with the possibility of enforcing the periodic condition on the final slopes. A simplified algorithm is as follows:

Algorithm 1: Modified Gerchberg algorithm in which slope measurements are extended beyond the aperture. The gradients obtained are periodic over the domain and the rotational is as close to zero as possible on account of the measurement noise.

Input: WFS measurements: $\{s_x^0; s_y^0\}$

for $i = 1, 2, \dots, n_{\text{iter}}$. **do**

1: Fourier transform \rightarrow slopes in Fourier space

$$\tilde{s}_x^{i-1} = \mathbf{TF}\{s_x^{i-1}\}$$

$$\tilde{s}_y^{i-1} = \mathbf{TF}\{s_y^{i-1}\}$$

2: Phase reconstruction (filtering) followed by gradient computation

$$\tilde{s}_x^i = \tilde{\mathcal{G}}_x (\tilde{\mathcal{R}}_x \tilde{s}_x^{i-1} + \tilde{\mathcal{R}}_y \tilde{s}_y^{i-1})$$

$$\tilde{s}_y^i = \tilde{\mathcal{G}}_y (\tilde{\mathcal{R}}_x \tilde{s}_x^{i-1} + \tilde{\mathcal{R}}_y \tilde{s}_y^{i-1})$$

3: Inverse Fourier transform \rightarrow extended slopes in direct space

$$s_x^i = \mathbf{TF}^{-1}\{\tilde{s}_x^i\}$$

$$s_y^i = \mathbf{TF}^{-1}\{\tilde{s}_y^i\}$$

4: Replace gradients within the pupil by the original measurement, keeping extrapolated gradients outside the pupil

$$s_x^i = s_x^0 P + s_x^i \bar{P}$$

$$s_y^i = s_y^0 P + s_y^i \bar{P}$$

5: If required the periodic condition is then enforced

if $P_{\text{cond.}} == \text{true}$ **then**

$$s_x(m, N) = -\sum_{n=1}^{N-1} s_x(m, n)$$

$$s_y(N, n) = -\sum_{m=1}^{N-1} s_y(m, n)$$

Output: Gradients over a $N \times N$ computational grid

Whilst with enough iterations ($n_{\text{iter.}}$) the Gerchberg routine will result in extended slope data which satisfies the periodic nature of the FFT the Hudgin extension requires explicit enforcement of the periodic condition (using the approach described in Eq. (5)), as this method of extending only the values at the aperture edge does not satisfy periodicity. The slopes initially generated through the Gerchberg routine are the result of an FFT and will therefore satisfy the conditions of the FFT (step 3 of the algorithm). The replacement of the data within the pupil by the original measurement results in a new set of non-periodic slopes (step 4), but with enough iterations the data will conform to a periodic data set. If a large number of iterations are required the periodic condition can be explicitly enforced as with the Hudgin extension.

Figure 1 shows an example of the Gerchberg extension (right) compared to the Hudgin extension (middle) and the original slope measurement (left). The Gerchberg extension exhibits a more gradual change in data across the boundary imposed by the aperture, whilst both the original slopes and Hudgin extended slopes contain sharper features.

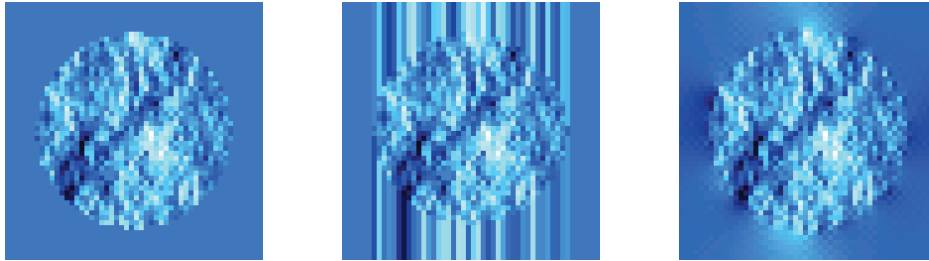


Fig. 1. Examples of different extension methods. **Left:** Original x slopes. **Middle:** x slopes extended using Hudgin extension method. **Right:** Extended x slopes using the Gerchberg method with 3 iterations. The examples are shown here before/without the imposition of the periodic condition.

The use of the Gerchberg routine will result in an increase in the number of operations. For each set of slopes the number of operations for the reconstruction process are as follows:

$$N_{\text{op.}} = \underbrace{n_{\text{iter.}} (2N \log(N) + 3N)}_{\text{Gerchberg algorithm}} + \underbrace{2N \log(N) + N}_{\text{Final reconstruction}} \quad (8)$$

where $n_{\text{iter.}}$ is the number of Gerchberg iterations and N is the number of system modes (or number of grid points). The $2N \log(N)$ terms refer to the forwards and backwards FFTs (in both the Gerchberg algorithm and final reconstruction). In the Gerchberg algorithm the $3N$ operations refer to the phase reconstruction, the gradient computation and the replacement of the original measurement, whilst the final reconstruction term only includes one N term for the phase reconstruction. This equation should be compared with the standard number of operations for a direct space matrix vector multiply method (MVM), N^2 . In Fig. 2 the number of operations for FFT reconstruction and MVM reconstruction are compared, with and without application of the Gerchberg method. Even with a large number of iterations of the Gerchberg algorithm ($n_{\text{iter.}} = 10$) the FFT reconstruction will offer a significant reduction in the number of operations required for ELTs (> 2 orders of magnitude with a small number of iterations).

We envisage the possible advantages of the Gerchberg method as producing more accurate results in both open and closed loop. However, if a large number of iterations are required this will increase computing time, diminishing the increase in speed offered by the FFT, whilst also adding another layer of complexity to the reconstruction process, providing greater possibility for noise propagation through the algorithm.

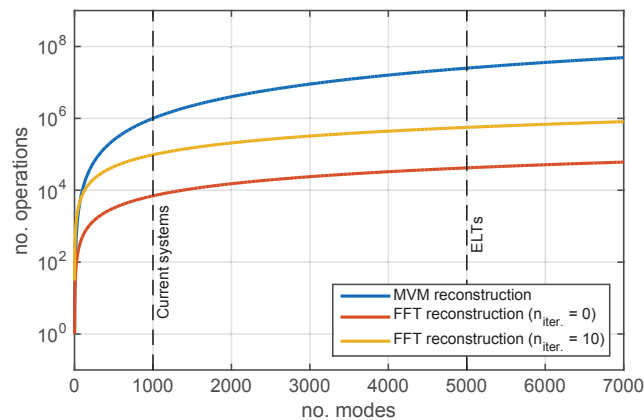


Fig. 2. Plot illustrating the number of operations required for wave-front reconstruction of an N mode system, both in direct space ($N \times N$) and for possible FFT reconstruction (see Eq. (8)). For FFT reconstruction two cases are shown, one without the Gerchberg extension ($n_{\text{iter.}} = 0$) and one with 10 Gerchberg iterations ($n_{\text{iter.}} = 10$). The state for current systems and ELTs are highlighted, showing the potential for a 1 – 2 order of magnitude reduction in the number of operations using Fourier methods.

4. End-to-end simulation results

In order to test the performance of the Gerchberg extension we compare the results of end-to-end simulations using our extension method and the Hudgin extension. Particularly we aim to investigate the number of iterations required to achieve a comparable performance, the impact of enforcing periodicity with the Gerchberg extension and the effect of the extension window (number of pixels either side of the aperture).

The results presented here are for a SPHERE-like case [18] and the parameters used are summarised in table 1. The simulations are carried out using OOMAO (Object Oriented Matlab Adaptive Optics toolbox) a MATLAB based simulation code [19]. The performance is quantified in terms of the spatial frequency content of the residual phase, the Strehl and noise propagation (as defined in [20]). The performance is compared for both open and closed loop cases and for simplicity a deformable mirror is not included (to separate DM fitting errors from the impacts of the different extension methods). The simulated atmosphere includes higher spatial frequency components than those defined by the lenslet spacing and therefore, with the omission of the spatial filter present in the SPHERE system, the simulations will include aliasing errors.

In all cases presented here the filter used for the final phase reconstruction and within the Gerchberg algorithm is the Rigaut filter, as detailed in [8]. The extension of the slopes data is carried out using three different methods:

1. The Gerchberg extension.
2. The Gerchberg extension with periodic condition enforced (using Eq. (5)).
3. The Hudgin extension (always enforces periodic condition).

Table 1. Summary of simulation parameters used in end-to-end simulations of a full AO loop. The atmospheric properties (the Fried parameter r_0 and outer scale L_0) are both given, as well as the telescope properties and wavelengths for the wave-front sensing and science star. The parameters correspond to a SPHERE-like system with the omission of the spatial filter before the WFS [18].

Parameter	Value
r_0	15 cm
L_0	30 m
No. atmosphere layers	3
Telescope diameter	8 m
No. lenslets	40
No. pixels per lenslet	6
λ_{WFS}	V band
$\lambda_{\text{sci.}}$	K band
Read-out noise	$2 e^-$
Guide star magnitude	8
Median wind speed	10 ms^{-1}
Sampling frequency	1 kHz

4.1. Open loop

Firstly we consider the open loop case. When no extension method is applied the errors caused by the aperture and non-periodic nature of the slope measurement result in a low Strehl ratio of 25.3% in K band. This can be compared to a theoretical Strehl of $\sim 97\%$, estimated using the Marechal approximation and including fitting and aliasing errors [21].

Figure 3 shows the Strehl ratio obtained using the Gerchberg extension versus iteration. The results are shown for different extension windows ($n = 3$ and $n = 6$ pixels) as well as with and without enforcement of the periodic condition (see Sec. 3.2 and [9]). Results using the Hudgin extension are also shown. With enough iterations all instances of the Gerchberg extension perform better than the Hudgin extension. However, enforcing periodicity on the data is crucial to achieving a good Strehl within a limited number (1 or 2) Gerchberg iterations. Without this the system takes significantly more iterations to converge.

A peak in performance using the Gerchberg routine is observed (i.e. at 2 iterations with the periodic condition). Additional iterations then result in a slight drop in Strehl. This can be the consequence of trying to fit the measured data to our model (the Fourier filters) through successive iterations, where the filters are not an exact match to the true measurement process. Another factor is an increase in noise propagation with additional iterations, as discussed in more detail below.

Figure 3 also reveals a difference in performance depending on the size of the extension window ($n = 3$ and $n = 6$). We observe this even in the case of no slope extension (i.e. 0 Gerchberg iterations corresponds to padding the original data with zeros). When the periodic condition is enforced the Strehl is already significantly improved. Without the periodic condition the Strehl is $\sim 30\%$ ($n = 3$) and $\sim 35\%$ ($n = 6$) compared to 25.3% for the non-extended case. The impact of the extension window is discussed in greater detail in Sec. 4.2.

Although enforcing periodicity results in a greater Strehl with fewer iterations the consequence is an error at higher frequencies, specifically near the waffle frequency ($\frac{1}{2d} = 2.5 \text{ m}^{-1}$). This is illustrated in the power spectral densities (PSDs) of the residual phase shown in Fig. 4. For the case with no extension (red trace) the PSD shows a relatively high low frequency content. This is

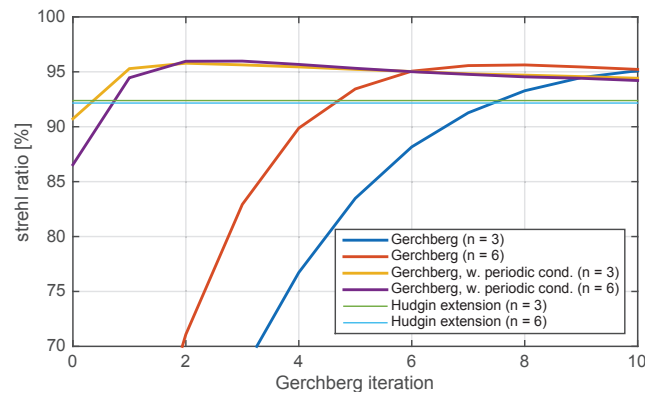


Fig. 3. Plots of the K-band Strehl ratio versus Gerchberg iteration for open loop end-to-end simulations. The results for 2 different extension windows ($n = 3$ and $n = 6$) are shown for 3 extension methods: 1) Gerchberg extension with enforced periodicity; 2) Gerchberg extension without enforced periodicity; and 3) the Hudgin extension.

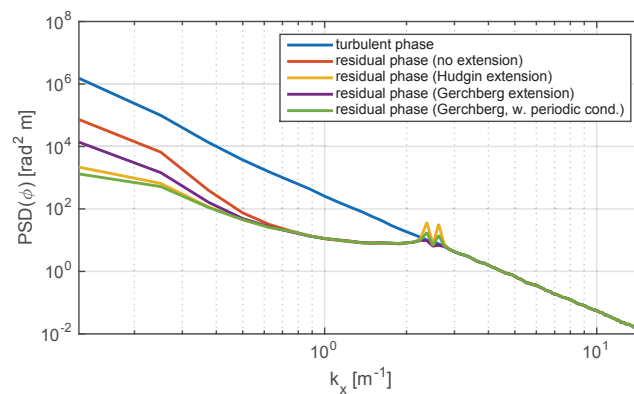


Fig. 4. PSDs (power spectral densities) of the turbulent phase and residual phase for different open loop simulations. In all cases the phase is reconstructed in the Fourier domain using different extension methods: 1) no extension; 2) Hudgin extension; 3) Gerchberg extension (3 iterations); and 4) Gerchberg extension with periodicity enforced (3 iterations). In the 3 extension cases (2–4) an extension window of $n = 3$ is used.

the result of the cut-off imposed by the telescope aperture: large errors in the estimation of the low spatial frequencies. The 3 extensions shown here all improve on the case with no extension. The two Gerchberg cases here use 3 iterations, in order to compare performance for a sufficiently low number of iterations. In the two cases where periodicity is enforced (the Hudgin extension and Gerchberg case) the low spatial frequency content is significantly reduced compared to the no extension case, with the Gerchberg extension doing slightly better than the Hudgin. This is reflected in a significant improvement in Strehl. However, at high spatial frequencies ($\sim 2.5 \text{ m}^{-1}$) there is a small error in the reconstruction. This is a result of enforcing periodicity along a single row/column of the slopes data, introducing a high spatial frequency element. This is not present in the Gerchberg case where periodicity is not enforced. However, as discussed above, it is not desirable to use the large number of iterations required for high Strehl when periodicity is not enforced in the Gerchberg extension. The cost of optimising the overall performance (the Strehl)

using the periodic condition is a small high spatial frequency error. Such errors can then be filtered out of the reconstructed phase using a specific filter [9, 10]. In addition the DM will provide some additional correction at these high frequencies [8].

In addition to an improvement in Strehl the Gerchberg extension also offers an improvement over the Hudgin extension in terms of noise propagation, as illustrated in Fig. 5. Here the error propagation coefficient (as defined in [20]) versus Gerchberg iteration is plotted, showing the improved performance of the Gerchberg. The inclusion of the periodic condition does slightly increase the propagation factor, as do the number of iterations. Again we conclude in support of enforcing periodicity, as although the noise propagation is higher for the same number of iterations we would require a large number of iterations without this condition to reach an acceptable Strehl, resulting in a similar noise propagation but increased computation time.

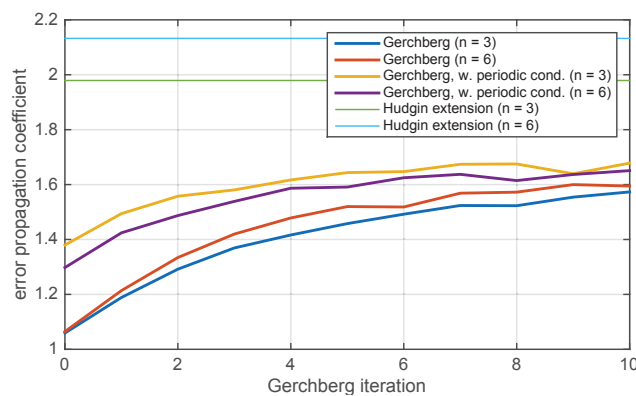


Fig. 5. Error propagation coefficient versus Gerchberg iteration for different extension methods and extension windows (n).

4.2. Closed loop

In closed loop the residual phase is estimated, allowing for smaller errors in the Fourier reconstruction due to the small nature of the aberrations. In the closed loop simulations presented here the Strehl is measured once the AO loop is closed, using a camera exposure of 200 closed loop time steps. Simulating a closed loop case results in a Strehl of 81.6% when no extension method (or extension window) is applied. The results in, terms of Strehl, for different extension methods are summarised in Fig. 6.

In closed loop the Gerchberg delivers a greater Strehl than the Hudgin extension and tends towards a high Strehl of $\sim 97\%$, close to the estimated Strehl. Temporal errors are included and the estimation involves knowledge of the closed loop transfer function and time delay of the system [22] (1 frame delay in this case). Unlike in open loop the number of iterations required for a stable Strehl both with and without the periodic condition is small (1 or 2). This is due to the nature of the closed loop, which itself is iterative in nature, applying the filtering process to the residual slopes. In this way the larger errors seen in open loop disappear.

In closed loop the application of the periodic condition in the Gerchberg actually causes a slight drop in performance. The periodic constraint identified in Sec. 3.3 is true for a no noise system of continuous (or concurrent) gradient measurements. The discrete measurement process of the Shack-Hartmann leads to the gradient of the average phase for each lenslet which, due to the discrete measurement of the WFS spots at the focal plane of each lenslet, is effectively taken across $d - d_{px}$, not the full sub-aperture (see Sec. 2). In this case the periodic condition is not the exact solution for a periodic phase. In closed loop the Gerchberg extension (without the

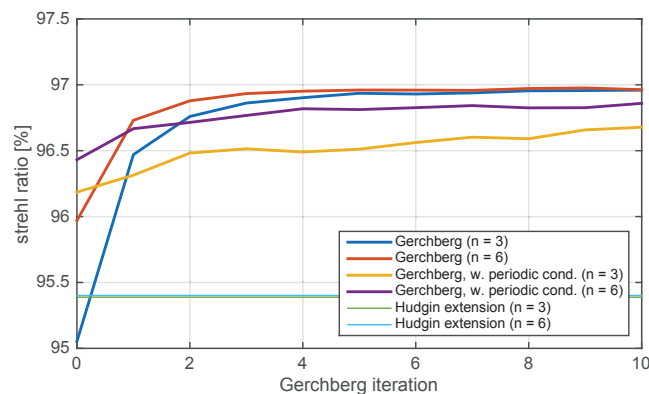


Fig. 6. Plots of Strehl ratio versus Gerchberg iteration for closed loop simulations. The results shown are for two different extension windows (n) and 3 different extension methods: 1) the Gerchberg extension; 2) the Gerchberg extension with periodicity enforced; and 3) the Hudgin extension.

periodic condition) requires only a few iterations to produce a consistent set of slope data, which due to the nature of the FFT are periodic. Enforcing the periodic condition is redundant and will add a high frequency element to the data not representative of the measurement, shifting the data away from its optimal extension and introducing a slight error into the reconstruction. Forgoing the periodic condition achieves a greater Strehl after 1 iteration, allowing for maximising the Strehl whilst avoiding the high frequency errors observed in open loop (see Sec. 4.1). Therefore for closed loop operation the periodic condition is not required.

As well as the increase in performance from the slope extensions we again observe an increase in performance (in terms of Strehl) purely by increasing the size of the reconstruction window (i.e. padding the slope data with zeros). This is illustrated in Fig. 6 by the results for the Gerchberg method with 0 iterations. In these cases the slopes have not been extended but the grid size has increased (by $n = 3$ and $n = 6$ points on both sides of the original data). An increase in Strehl compared with the non-extended case (81.6%) is observed. As shown in Fig. 4 the errors induced by the aperture are predominantly low spatial frequency errors. Increasing the size of the window shifts these errors into the low spatial frequencies defined by the new window and out of those defined by the measurement data. Further extension of the window (with and without enforced periodicity) tends to a maximum Strehl of $\sim 96.5\%$ but does not reach the optimal performance offered by the Gerchberg extension. In addition the results with zero padding exhibit greater noise propagation and the development of unstable waffle-like modes (as discussed in greater detail below).

In addition to the improvements in Strehl offered by the Gerchberg the closed loop performance also demonstrates a reduced error propagation compared to other extension methods. These results are shown in Fig. 7. Again, as with the open loop results, the error propagation increases with iteration and with the addition of the periodic condition. For the closed loop however, we do not require the periodic condition to maximise the Strehl with few iterations and so the Gerchberg extension is optimal both in terms of Strehl and error propagation.

The iterative process of the closed loop can result in small errors in the reconstruction process propagating through the loop and producing large unstable modes. In a standard Shack-Hartmann system these unstable modes are commonly the waffle modes. In the closed loop results presented here we consider exposures of 200 time steps. When using the Hudgin extension for longer exposures the beginnings of unstable behaviour were observed, even with the application of

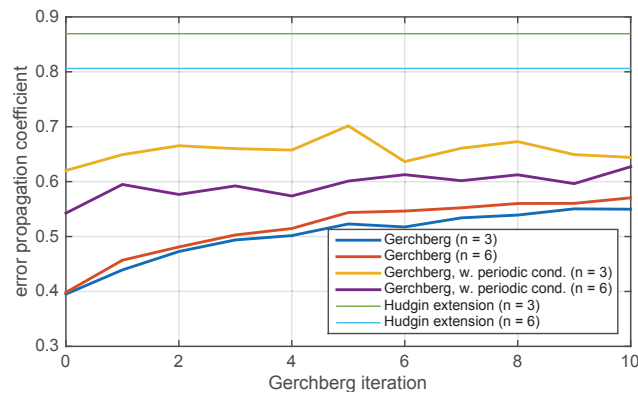


Fig. 7. Error propagation coefficient versus Gerchberg iteration for different extension methods and extension windows (n) in end-to-end closed loop simulations.

global and local waffle filters. This is illustrated in Fig. 8 where the short exposure Strehl for each time step of the closed loop is plotted for different extension methods. In this case we also include a comparison with another extension method, the edge correction method [13], which only extends the slopes into the data points immediately adjacent to the aperture. In comparison with these two methods the Gerchberg demonstrates very stable behaviour, even without the application of the waffle filters. Although the results presented here use the Rigaut filter for phase reconstruction additional tests carried out using the *Hudgin filter* [8] with the Hudgin extension in closed loop demonstrated similar results and unstable behaviour. This issue of instability for the Hudgin and edge extension methods could be further addressed by optimising the gain for each individual mode [13]. However, the optimisation of these extensions is not the subject of this paper.

The edge method was not presented as the comparison method in this paper due to the better overall performance (in terms of Strehl) of the Hudgin extension (as shown in Fig. 8). However, the edge extension demonstrates a less noisy behaviour, compared to the Hudgin extension, whilst still being effected by the development of unstable modes over time. We can conclude

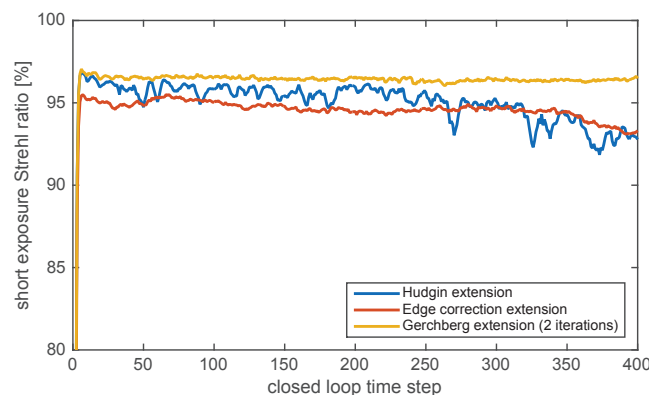


Fig. 8. Short exposure Strehl ratio vs. closed loop time step for 3 different extension methods: 1) Hudgin extension; 2) edge correction extension [13]; and 3) Gerchberg extension (2 iterations). In all cases the local and global waffle modes have been filtered out.

that although there are other methods with the potential to increase the Strehl (increasing the extension window) or provide a more stable/less noisy closed loop performance (edge extension) the Gerchberg extension is the only method which optimises both and provides a very stable performance.

Finally we consider the PSFs simulated for the different extension methods in order to further compare the performance. Figure 9 shows the PSFs generated over an exposure of 200 closed loop time steps for the Hudgin extension (left) and 2 iterations of the Gerchberg extension (right). Only the corrected region is shown. The centre of the PSF appears similar for both cases. However, the Gerchberg extension demonstrates an improved contrast towards the edge of the correctable band, in the $10 - 20 \frac{\lambda}{D}$ region and particularly in the corners. This corresponds to errors at high spatial frequency, particularly waffle-like modes.

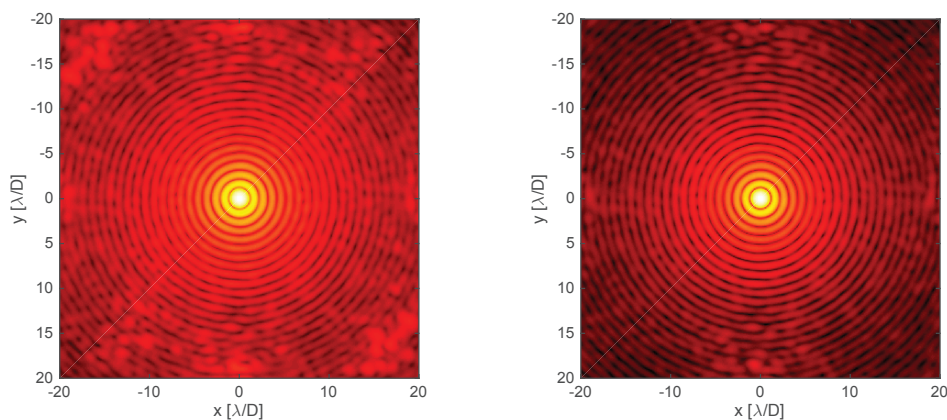


Fig. 9. Closed loop PSFs for Fourier reconstruction using different extension methods. **Left:** Hudgin extension. **Right:** Gerchberg extension with $n_{\text{iter.}} = 2$. Only the corrected region is shown and the same colour scheme is used for each image.

5. Conclusions

We propose a method for extending wave-front sensor data outside of the aperture imposed by the telescope pupil based on an iterative Gerchberg routine. Expanding on the work of Roddier&Roddier [7] this extension method involves recursive Fourier reconstruction of the phase across a rectangular domain, extrapolating the slope measurements outside the bounds of the aperture. The development of this extension method was motivated by a desire to achieve improvements in Fourier wave-front reconstruction using anti-aliasing filters derived in [8]. The Gerchberg method avoids some of the spatial frequency errors and instabilities observed in other methods, allowing the full potential of such filters to be realised.

Demonstration of this technique using end-to-end simulations has shown improved performance over other extension methods. In open loop an increase of $\sim 3\%$ Strehl (in K-band) over previous methods is achieved, whilst noise propagation is reduced. Such improvement can be achieved with minimal iterations of the Gerchberg (1-2) when a periodic condition is enforced. In closed loop gains in Strehl of $\sim 1.5\%$ and a similar reduction in noise propagation are observed, when compared with previous methods. In the case of closed loop operation the periodic condition is not required to optimise performance with 1-2 iterations and the Gerchberg method also exhibits extremely stable behaviour over time. This corresponds to significant gains in rms (~ 40 nm) and an increase in contrast for the final PSF ($10 - 20 \frac{\lambda}{D}$). This shows great

potential for the development of such methods for future high-contrast imagers, such as SPHERE 2.0.

The disadvantage of the Gerchberg method is the iterative process, which will increase the computation time. However, we require a limited number of iterations: in both open and closed loop a single iteration improves performance on existing methods. For a single reconstruction process of an N mode system the number of operations will be $n_{iter} \cdot (2N \log(N) + 3N) + 2N \log(N) + N$, where n_{iter} is the number of Gerchberg iterations, compared with N^2 operations for standard direct space reconstructors. With the small number of iterations required the increase in speed provided by the FFT is preserved and we can expect a reduction in the number of operations greater than 1 order of magnitude for future large AO systems.

Using the Gerchberg method we also anticipate further advantages due to the ability to replicate the properties of the WFS measurements outside the aperture without the sharp features introduced by other extension methods. This avoids introducing additional features to the reconstructed phase, leading to errors particularly at high spatial frequency. Here we have presented results as applied to apertured data, but this method is potentially applicable to other obstructions. For example segmented telescopes, such as future ELTs, will produce spatially discontinuous WFS data. We foresee the use of the Gerchberg method to extend the slope data between the segments, thus allowing for reconstruction using Fourier methods. In addition the Gerchberg formalism should be directly applicable to other types of wave-front sensor, such as the Pyramid, whose signals are not pure gradient measurements and so do not conform to previously derived constraints. Further investigations into this method may also prove useful for the application of Fourier reconstruction over non-cartesian grids, such as the actuator geometry proposed for the European Extremely Large Telescope system HARMONI [23].

Funding

A*MIDEX project (no. ANR-11-IDEX-0001- 02) funded by the Investissements d’Avenir French Government program and managed by the French National Research Agency (ANR); Cco-funded by the People Programme (Marie Curie Actions) of the European Union’s Seventh Framework Programme (FP7/2007-2013) under REA grant agreement n; PCOFUND-GA-2013-609102, through the PRESTIGE programme coordinated by Campus France.

Acknowledgments

All simulations presented are done using the object-oriented MALTAB AO simulator (OOMAO) [19] freely available from <https://github.com/cmcorreia/LAM-Public>.